



Characterization of surface oil thickness distribution patterns observed during the Deepwater Horizon (MC-252) oil spill with aerial and satellite remote sensing



Jan Svejkovsky^{a,*}, Mark Hess^a, Judd Muskat^b, Tim J. Nedwed^c, Jenifer McCall^a, Oscar Garcia^d

^a Ocean Imaging Corp., 13976 West Bowles Ave, Suite 100, Littleton, CO 80127, United States

^b Office of Spill Prevention and Response, California Dept. of Fish and Wildlife, 1700 K Street, Suite 250, Sacramento, CA 95811, United States

^c Exxon Mobil Upstream Research Company, 22777 Springwood Village Parkway, Spring, TX 77339-1425, United States

^d Water Mapping, LLC, Tallahassee, FL, United States

ARTICLE INFO

Article history:

Received 1 March 2016

Received in revised form 31 May 2016

Accepted 17 June 2016

Available online 4 July 2016

Keywords:

Oil spill

Remote sensing

Oil thickness distribution mapping

Deepwater Horizon

Subsea dispersants

ABSTRACT

Knowledge of the spatial distribution of oil thickness patterns within an on-water spill is of obvious importance for immediate spill response activities as well as for subsequent evaluation of the spill impacts. For long-lasting continuous spills like the 2010 3-month Deepwater Horizon (DWH) event in the Gulf of Mexico, it is also important to identify changes in the dominant oil features through time. This study utilized very high resolution (≤ 5 m) aerial and satellite imagery acquired during the DWH spill to evaluate the shape, size and thickness of surface oil features that dominated the DWH slick. Results indicate that outside of the immediate spill source region, oil distributions did not encompass a broad, varied range of thicknesses. Instead, the oil separated into four primary, distinct characterizations: 1) invisible surface films detectable only with Synthetic Aperture Radar imaging because of the decreased surface backscatter, 2) thicker sheen & rainbow areas (< 0.005 mm), 3) large regional areas of relatively thin, “metallic appearance” films (0.005–0.08 mm), and 4) strands of thick, emulsified oil (> 1 mm) that were consistently hundreds of meters long but most commonly only 10–50 m wide. Where present within the slick footprint, each of the three distinct visible oil thickness classes maintained its shape characteristics both spatially (at different distances from the source and in different portions of the slick), and temporally (from mid-May through July 2010). The region over the source site tended to contain a more continuous range of oil thicknesses, however, our results indicate that the continuous injection of subsurface dispersants starting in late May significantly altered (lowered) that range. In addition to characterizing the oil thickness distribution patterns through the timeline of one of the world's largest oil spills, this paper also details the extension of using high resolution aerial imagery to calibrate medium resolution satellite data sources such as USA's Thematic Mapper (30 m) to provide larger-scale spatial views of major spills, and discusses implications for utilizing such data for oil spill characterizations and spill response.

© 2016 Elsevier Ltd. All rights reserved.

1. Introduction

Timely information about the spatial extents of an at-sea oil spill and the distribution of oil thickness patterns within it is very important for planning and managing immediate response activities. A common rule-of-thumb for marine oil slicks is that 90% of the oil exists in 10% of the area. Traditional aerial visual observations by trained observers cannot distinguish oil thicker than the black oil that forms when slicks become approximately 0.1 mm thick.

Efficient allocation of response resources using vessels, booms and skimmers depends on knowing which parts of the slick contain the most recoverable oil. Likewise, successful in-situ burning and aerial or vessel-based dispersant application planning requires knowledge of both the relative thickness and weathering/emulsification states of the

potential oil targets. This intelligence is traditionally obtained through visual observations from fixed-wing and rotary aircraft, however, these are being increasingly augmented by satellite and aerial remote sensing.

The majority of marine oil spills are of the “batch” variety where a finite amount of petroleum is released during an event lasting a few hours (e.g. from a ruptured tank vessel or pipeline that is quickly shut down). The released oil undergoes evaporation, drift due to currents and winds, dispersion from waves, entrapment of water droplets (emulsification), UV and biological degradation, etc. that affect its spatial extents and thickness patterns. Over time, oil from batch releases tends to reflect the same advanced weathering parameters. “Continuous” spills, where fresh oil is released over long periods, are very uncommon relative to “batch” spills. Although the same weathering and advection parameters affect the discharged petroleum in both types of spills, the continuous discharge spill differs in that it usually lasts for a significantly longer time period, with both freshly discharged oil and

* Corresponding author.

E-mail address: jan@oceani.com (J. Svejkovsky).

extensively weathered oil being simultaneously present within the slick through the event. The spatial distribution of thickness and weathering state of oil features from a continuous spill and any potential temporal changes in such patterns through the extended spill period has not previously been studied. Such knowledge could advance better preparedness for response strategies in future large spills.

On 20 April, 2010 the Deepwater Horizon (DWH) oil rig exploded in the Gulf of Mexico and continued to spill oil into the sea until 15 July 2010 when the wellhead was finally capped. The spill was the largest accidental spill and second largest in history, exceeded only by the Mina al Ahmadi spill during the first Gulf War in 1991 (NOAA, 2011). Due to the size of the spill, traditional visual aerial surveys could not provide complete coverage of the spill area on a daily basis. As part of the response, multiple remote sensing technologies and sensors were mobilized. The most frequently utilized data during the response were provided by Synthetic Aperture Radar (SAR) sensors, and Side-Looking Airborne Radars (SLARs) flown by Transport Canada and Icelandic Coast Guard, which were used to render the full extents of the oil slick (regardless of thickness) and their changes in time. Very high resolution multispectral visible and thermal infrared aerial imagery flown by USA's Ocean Imaging Corporation (OI) was acquired near-daily over selected parts of the slick and was used to provide, for the first time, operational maps of oil thickness distributions over the imaged areas (Svejkovsky et al., 2012A). (Several other aerial imagers, both federal and corporate, collected data primarily for research, test or baseline documentation purposes but were not deployed on a routine, daily basis and did not provide the imagery to aid daily response activities.) Limited numbers of cloud-free images were also collected with various commercial high resolution optical satellites such as Digital Globe's WorldView-2 (WV-2), and medium-resolution satellites such as France's SPOT and USA's Landsat Thematic Mapper (TM). Coarse resolution satellite imagers such as USA's Moderate Resolution Imaging Spectroradiometer (MODIS) aboard National Aeronautics and Space Administration's (NASA's) Aqua and Terra satellites provided near daily coverage of the spill in the visible, near-IR and thermal-IR bands at resolutions of 255–1000 m.

The volume of remote sensing data collected from these sources and their daily application during the lengthy spill represents to-date the most intense utilization of remote sensing technologies during an oil spill incident. Although all the aerial and very high resolution satellite image sources captured only portions of the extensive spill slick on a particular day, they are sufficiently varied in space and time to provide representative data with very fine detail from different parts of the slick area throughout the event timeline. This paper describes results of a study utilizing this unique high and medium resolution imaging archive to characterize the spatial and temporal distribution of oil thickness patterns within the DWH slick, and effects on those distributions by major natural (Tropical Storm Alex) and anthropogenic (subsurface dispersant injections) events during the 3-month spill.

2. Materials and methods

2.1. Principles of crude oil on water characterization

The presence of a floating crude oil film alters the sea surface's reflectance, emittance and radar backscatter characteristics in the visible-nearIR, thermal IR, and microwave portions of the electromagnetic spectrum respectively. The alterations provide a means to detect and in some cases quantify the presence and thickness of the oil film with various aerial and satellite remote sensing instruments. Numerous review articles summarize the underlying principles (e.g. Brekke and Solber, 2005; Jha et al., 2008; Fingas and Brown, 2011; Leifer et al., 2012) and, in the last few years, the volume of both laboratory and operational research on the subject has been steadily increasing. For the purposes of this study we summarize here only the core properties that allow easily verifiable distinction between crude oil sheens, thin

and thick fresh oil films, and emulsified oil accumulations with combined use of SAR, multispectral visible-nearIR, and thermal IR sensors.

Crude oil spilled on open water tends to spread out very quickly. The thinnest layers are referred to as “sheens”. For our purposes, we adopt NOAA's definition of this term, which encompasses thicknesses from the thinnest, near-monomolecular, to grey/silver, to rainbow-appearing films (NOAA, 2012). This category thus includes films up to approximately 5 μm in thickness (Bonn Agreement, 2007, NOAA, 2012). The presence of sheens tends to increase reflectance in the ultraviolet range (Grüner et al., 1991). Because even very thin sheens suppress capillary waves on the sea surface, they suppress the microwave backscatter return from SAR sensors, making such instruments very sensitive to oil film detection (Gade et al., 1998; Minchew et al., 2012). All sheens are transparent in the visible wavelength region and, except for the silver and rainbow-appearing ones, tend to alter the underlying water color to a minimal degree, making their detection with visible-wavelength sensors a function of the instrument's sensitivity and signal-to-noise ratio. As is discussed below, during the DWH spill OI's 12-bit aerial sensor was able to detect “silver” and thicker sheens (i.e. approximately $>0.2 \mu\text{m}$), primarily due to increased reflectance (relative to surrounding water) in the 451 nm channel. The 8-bit TM satellite sensor, on the other hand, could reliably detect only the thickest rainbow sheens. Sheens also tend to be undetectable for the most part in thermal IR imagery. Their thermal detection is dependent on registering sufficient negative thermal contrast (due to petroleum's lower-than-water emissivity) to reliably separate them from surrounding water areas. Laboratory and open-sky test tank experiments have shown that even with very sensitive instruments, the minimum detectable oil film thickness is in the 10–20 μm range (Belore, 1982; Hurford, 1989; Svejkovsky et al., 2012A; Svejkovsky and Muskat, 2009). The thicker rainbow sheens tend to become detectable (both during day and night) by showing a decidedly cooler-than-surrounding-water signature.

Petroleum films thicker than sheens tend to appear, in the visible portion of the spectrum, as a combination of the underlying water color, sky reflectance and progressively more of the oil's dark brown/black “true color”. The color characterization of oil films just thicker than sheens has been subject to debate. Through its Bonn Agreement Oil Appearance Code (BAOAC), the European Union introduced the term “metallic” for oil films in the thickness range of 5–50 μm (Bonn Agreement, 2007). This terminology has also been more recently adopted by NOAA (NOAA, 2012). A distinguishing feature of metallic oil films is that they are transparent, making it possible to see submerged objects through them. Because of the transparency, a significant portion of the reflectance profile in the visible wavelengths parallels the profile of the surrounding water reflectance, a distinguishing feature in multispectral classification analysis. In thermal IR, the metallic thickness range films exhibit a negative thermal contrast signature, believed to be primarily due to the petroleum's lower emissivity relative to water (Shih and Andrews, 2008). The negative contrast can be $>1 \text{ }^\circ\text{C}$ and decreases with increasing thickness (Svejkovsky and Muskat, 2009). In SAR data the metallic thickness films are readily discernible due to their backscatter suppression, but are not distinguishable from sheens.

Crude oil films thicker than approximately 50 μm tend to progressively attain more of their natural dark brown/black color as less light gets reflected back through the film from the underlying water column. The Bonn Agreement refers to these thicknesses as “Discontinuous True Colors” (50–200 μm) and “True Colors” ($>200 \mu\text{m}$), and NOAA uses “Transitional Dark (True) Color” and “Dark (True) Color” labels. In the visible range crude oil films become completely opaque at approximately $>100 \mu\text{m}$ and no longer change their reflectance characteristics in multispectral imagery (Svejkovsky et al., 2008). They generally exhibit significantly reduced reflectance from the surrounding water signal, particularly in the blue and green wavelength range. During nighttime with no solar heat input, crude oil films thicker than 50 μm were found to retain a negative thermal contrast during summer air temperatures, which increased with increasing film thickness

(Svejkovsky and Muskat, 2009). During the daytime under both clear sky and cloudy conditions, however, the thermal signal of such films tends to show a positive thermal contrast, which increases with increasing thickness. This reversal has been observed by researchers in the past (Goodman, 1994; Tseng and Chiu, 1994; Byfield, 1998) and has been modeled (Shih and Andrews, 2008). It is due to the oil's higher absorption of solar heat input as the film becomes darker with increasing thickness. The actual oil thickness at which the reversal becomes evident in thermal-IR imagery varies somewhat, likely due to environmental conditions, oil composition, instrument sensitivity, etc., but for the purposes of this study, the existence of a positive thermal contrast exhibited by an oil target during daytime provides a high-confidence indication that its thickness is in excess of 50–70 μm . In SAR data such films are readily discernible from clear water areas due to their backscatter suppression, but are not distinguishable from sheens and metallic films.

Oil films floating on the sea surface are immediately subject to various degenerative processes commonly referred to as “weathering”. These include evaporation of the most volatile components (which can cause 30% or more reductions in volume within the first 24 h (Lehr et al., 2010)), dissolution, natural dispersion of small droplets into the water column, photodegradation, biodegradation, and emulsification. For the purposes of this study we separate emulsification from the other weathering phenomena, because unlike the others that tend to reduce the oil volume/thickness and change only somewhat its basic reflectance properties (such changes have not been well studied to-date), emulsification drastically alters the oil's reflectance, emittance and, in some cases, backscatter properties. Oil emulsions generally tend to represent the thickest oil films found in a spill event – in the DWH case field samples were documented to have thicknesses ranging from a few millimeters to several centimeters (Belore et al., 2011). The lower thickness limit of crude oil emulsions has not been clearly established, but with the water-in-oil droplet size often being on the order of a few microns, relatively thin films of truly emulsified oil are possible. To the naked eye stable, floating oil emulsions usually appear distinctly brighter than the original fresh crude, ranging from light brown to orange or red (hence red tides are sometimes mistaken for emulsified oil), and correspondingly exhibit high reflectance values in the longer wavelength bands of multispectral visible imagery. They also have high reflectance in the near-IR bands. In the DWH case, emulsions most commonly encountered tended to be orange and reddish. In daytime thermal-IR imagery emulsions appear either cooler or warmer than surrounding water, depending on a combination of their water content and thickness. Svejkovsky and Muskat (2012B) found that increasingly thicker emulsions containing 20% water had a contrast progression very similar to fresh oil, whereas emulsions containing 60% water required a thickness of 10 to 15 times that of fresh oil to exhibit the same contrast characteristics. In the DWH case field sampling done by Belore et al. (2011) most commonly showed water content in the 30–60% range. Recent analysis of time coincident OI's aerial imagery and very high resolution SAR imagery obtained during DWH has shown that very thick emulsions can sometimes be clearly discerned in SAR imagery due to their higher backscatter relative to surrounding water, fresh oil and thinner emulsion areas (Garcia-Pineda et al., 2013b).

2.2. SAR data processing

From April to August 2010, an extensive array of satellite and aerial sensors collected reflectance data on the surface of the ocean on a daily basis. Among all of the sensors, SAR was a key technology, both because it has a proven track record for detecting and quantifying marine oil spills (e.g., Garcia-Pineda et al., 2009) and because imagery was available nearly every day. Modern SAR satellites offer a number of advantages for the detection and monitoring of oil in the ocean. SAR sensor technology enables earth monitoring activities which are relatively independent of weather and sun illumination conditions (Alpers and Hühnerfuss, 1988). SAR images are acquired

day and night and through cloud cover, which is an advantage over other remote sensing sensors.

A semi-automated classification algorithm, the Textural Classifier Neural Network Algorithm (TCNNA) had been developed prior to the DWH spill specifically to delineate oil captured in SAR imagery (Garcia-Pineda et al., 2009). This algorithm was subsequently updated to process SAR imagery collected during the DWH event (Garcia-Pineda et al., 2013a, 2013b). The TCNNA semi-automated routine filters a grey-scale image (Fig. 1. left) with a variable boundary kernel size (regularly used is a 25×25 pixel kernel or larger depending on the spatial resolution) for edge and shape detections based upon the Leung-Malik filter bank (Garcia-Pineda et al., 2009, 2013a, 2013b). The neural network algorithm interpolates these detections within a training set previously compiled by the operator through classification of several thousand pixels from the same images under analysis.

Since the neural network classifier operates on a pixel basis, the TCNNA output maintains the original resolution of the SAR image. The resulting TCNNA binary output also preserves the original projection. The fully implemented TCNNA routine produces a georectified raster image in which all pixels have a binary classification of either floating oil or not floating oil. The result of this processing is an image that defines the slick outline. The defined slick is based on enough surface oil to inhibit capillary waves and therefore backscatter. That is, the slick could contain any oil thickness from an invisible sheen to thick emulsions. Fig. 1. (right) shows an example of the TCNNA classification (white outline). OI's DMSC/IR aerial image coverage acquired over different portions of the spill within 5 h of the SAR acquisition is also shown.

2.3. DMSC aerial system

During the DWH event, OI utilized its Digital Multispectral Camera (DMSC-MkII) imager manufactured by SpecTerra Ltd. in Australia. This frame-grabber type imager uses four lenses and 4 1024×1024 silicon-based CCDs to yield four data channels with 12-bit radiometric resolution. Each channel's wavelength range is customized with 10 nm-wide interference filters. The system was configured with three channels in the visible and one in the near-IR. The DMSC was coupled with a Jenoptik IR-TCM-640 (640×480) camera, providing one channel in the thermal-IR (see Table 1 for further specifications). In the offshore regions the system was flown at 12,500 ft altitude, yielding 2 m multispectral and 4 m thermal-IR resolution imagery.

OI had previously developed an oil film thickness determination algorithm utilizing image data from the DMSC/IR system. This algorithm was developed and validated over several years utilizing controlled experiments at the Bureau of Safety and Environmental Enforcement's outdoor Ohmsett facility in New Jersey, as well as field experiments utilizing natural oil seeps in Santa Barbara Channel, California (Svejkovsky and Muskat 2006, Svejkovsky et al., 2008; Svejkovsky and Muskat, 2009). The system was first used experimentally during the 2007 *M/V Cosco Busan* spill in San Francisco Bay, and then operationally during several spills in California such as the Platform A spill in 2008 (Svejkovsky et al., 2009). When the DWH event occurred, OI was contracted by BP at NOAA's request to provide aerial image acquisition and processing support for the response effort. OI conducted imaging flights with the DMSC/IR system near-daily (and sometimes twice daily) throughout the 3-month spill event beginning on 4 May 2010. The objective was to provide the incident command with oil thickness distribution analysis maps in near-real-time. Details of the system's use, thickness algorithm adaptation, results and lessons learned during the DWH effort are published in Svejkovsky et al., 2012A.

As mentioned above, the oil mapping system was previously used operationally on two spills in California. In both cases, the imaging required merely 1–5 flight lines of a few kilometers in length to completely image the spill-affected area. At 2 m resolution, the DMSC imaging swath is 2048 m and some overlap is required between adjacent

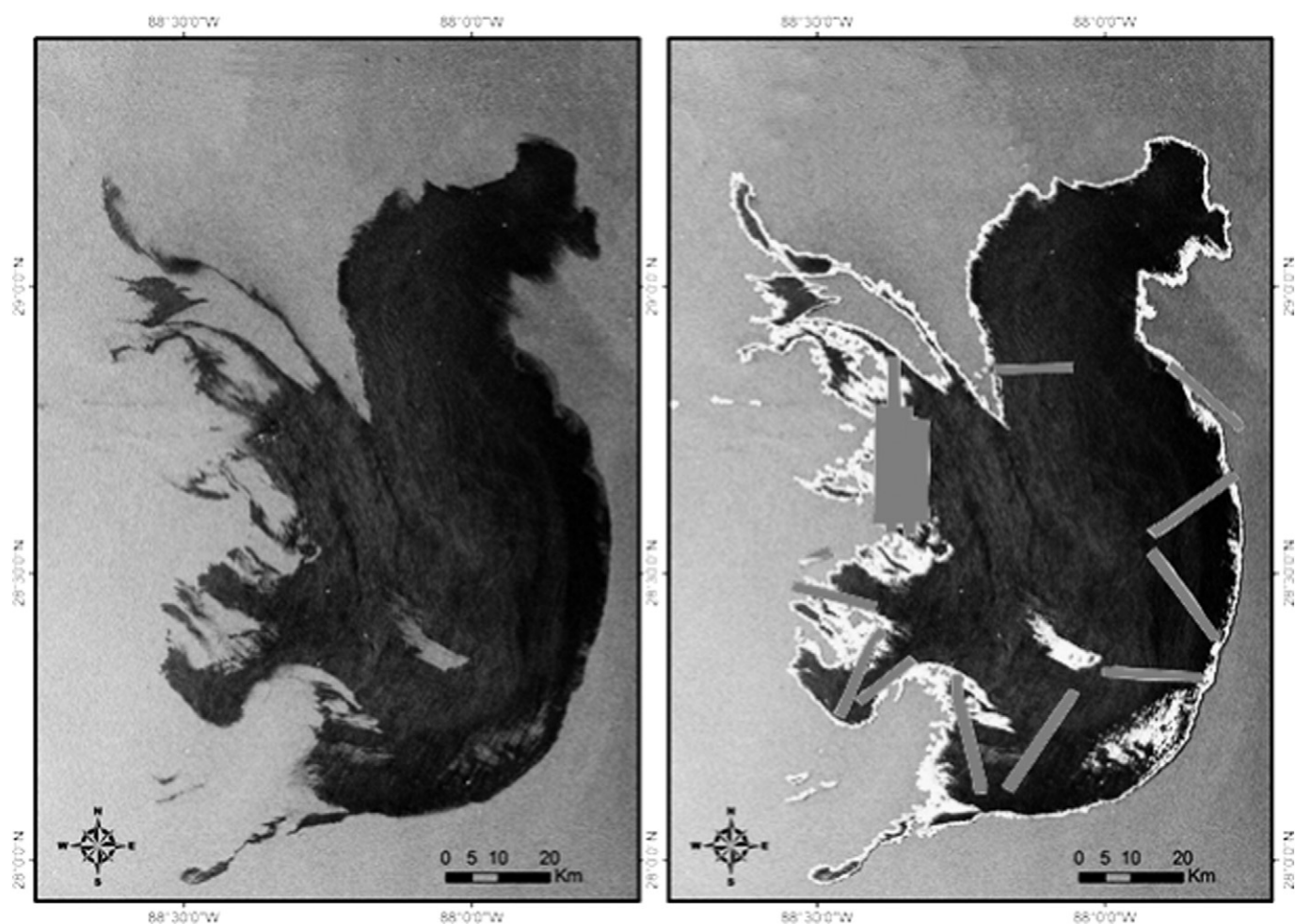


Fig. 1. Sample SAR image (left) and resulting TCNNA output (right). The RADARSAT-2 image was acquired on May 10, 2010 (23:53 UTC). The dark feature corresponds to surface oil films from the DWH spill. The segmentation produced by the TCNNA output is shown as a white outline of the entire spill footprint on the right. Also shown in grey are flight line areas of DMSC/IR multispectral imagery collected within 5 h of the SAR overpass.

image lines for proper multi-line mosaicking. Already on 4 May 2010 the size of the DWH spill precluded any attempts to map the complete spill area. Since sun glint severely degraded image usefulness of visible wavelength imagery from the DMSC sensor, imaging was limited to several hours in the morning after sunrise and several hours in the afternoon before sunset when low sun angles prevailed. (The thermal IR imagery is not affected by sun glint and could be used throughout the

day and night.) These spatial and temporal limitations dictated that the OI team received guidance on which specific target areas within the spill area to image each day. Initially such guidance and target area prioritization was received independently from the multiple Incident Command Centers (ICCs) that were established. Later in the spill, the Houma, Louisiana ICC became the lead center for guiding the various remote sensing missions.

Table 1

Spectral bands and characteristics of each sensor that were used for oil characterization analysis.

Sensor	Bands used (nm)	Resolution (m)	Dynamic range (bits/pixel)
DMSC/TIR	0.450	2	12
	0.551	2	12
	0.600	2	12
	0.710	2	12
	7.5–14	4	16
WV-2	0.400–0.450	2	11
	0.510–0.580	2	11
	0.585–0.625	2	11
	0.705–0.745	2	11
Spot 5	0.500–0.590	10	8
	0.610–0.680	10	8
	0.780–0.890	10	8
TM/eTM	0.450–0.520	30	8
	0.520–0.600	30	8
	0.630–0.690	30	8
	0.760/770–0.900	30	8

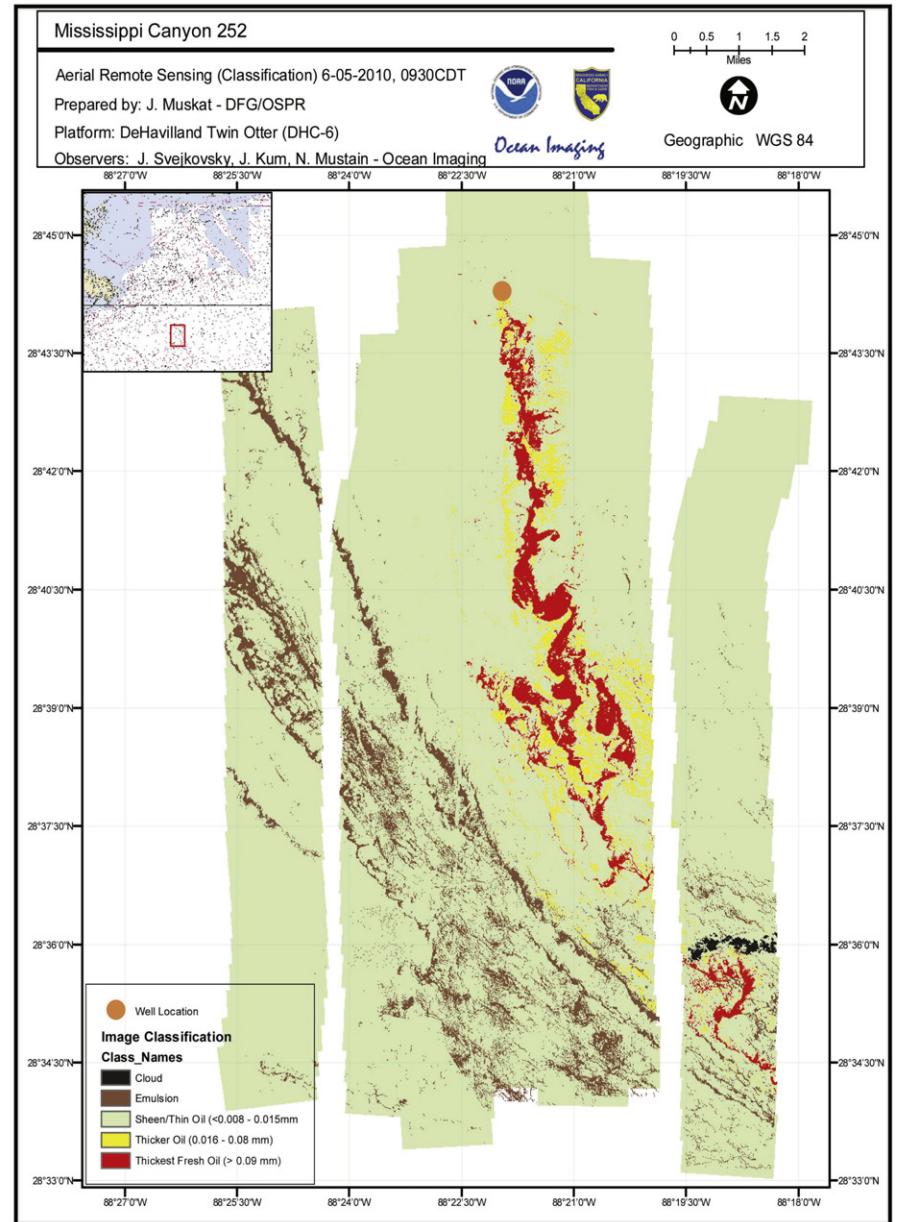
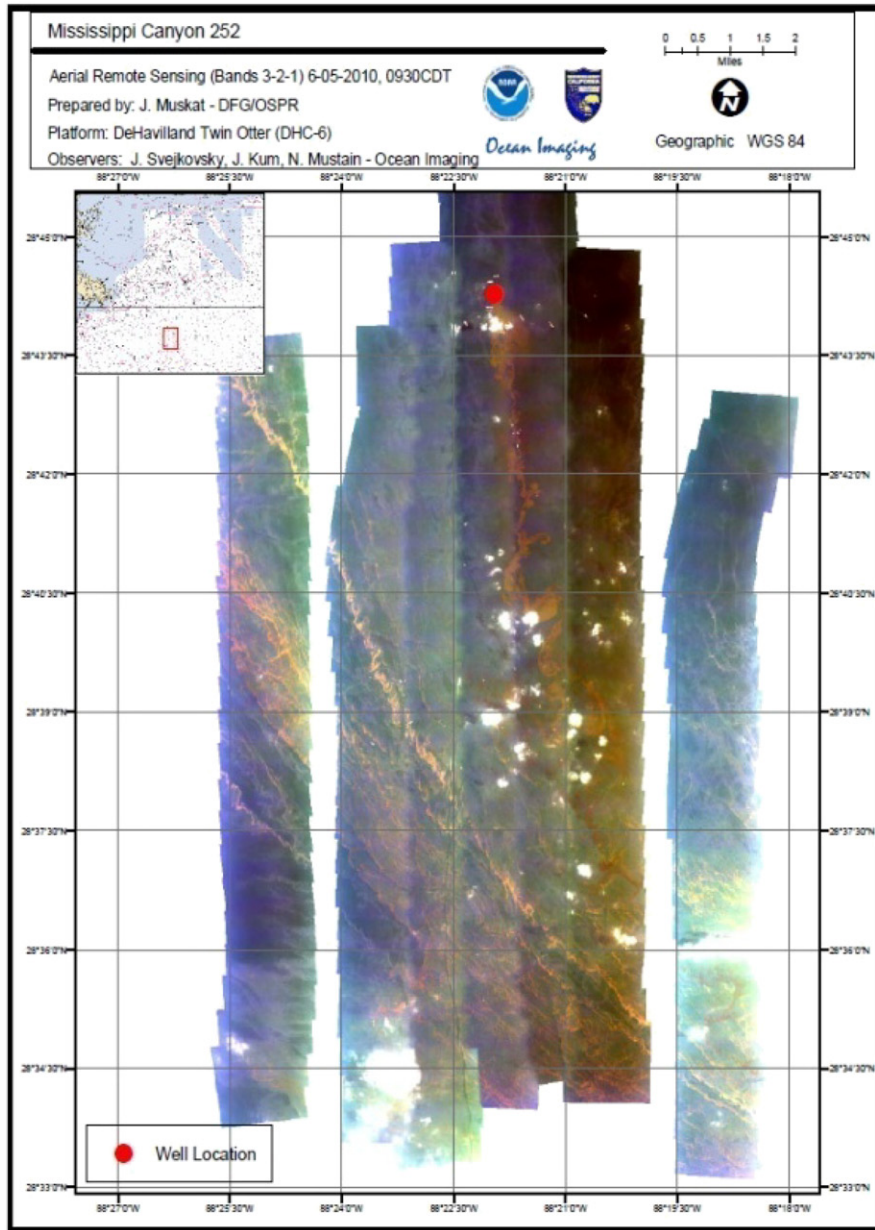


Fig. 2. DMSC/IR multispectral image mosaic of the DWH spill source plume region acquired on 6 May 2010 (left) and resulting oil thickness classification (right).

The oil thickness distribution analysis processing was hampered by data processing difficulties due to the extreme haze, sun angle and (on some flights) overhead cloud-caused illumination imbalances which affected the visible wavelength image quality. Flight takeoff timing (often at first light), length, and other logistics also prevented the collection of adequate pre-flight and in-flight calibration data that are normally used for standard application of the above-described oil thickness classification algorithm. These factors contributed to the need for additional, manual processing procedures to maintain quality control and flight-to-flight oil map product consistency. In order to maintain accuracy and day-to-day consistency under such conditions, OI modified the initial algorithm to bin the oil thickness determinations into only four or less thickness range classes. Additionally, since the algorithm was developed to determine thickness of freshly spilled oil, emulsified oil features were identified as such and included in a single “emulsion” class, regardless of thickness. An example of a typical daily oil thickness distribution analysis covering the DWH spill source site region is shown in Fig. 2.

2.4. World-view 2 and spot satellite data processing and calibration

In 2011, an image data set acquired by the World-View 2 (WV-2) satellite on 15 June 2010, encompassing approximately 323 km² was graciously provided to OI for experimental analysis for this study by Digital Globe Corporation. WV-2 has 8 bands in the visible-to-nearIR spectrum with approximately 2 m resolution – making its data directly comparable with those acquired by OI's DMSC aerial sensor. The WV-2 spatial coverage significantly exceeded that available with OI's aerial imaging. Our objective was to utilize the WV-2 data set to create an oil thickness classification product mimicking those created from OI's DMSC/IR imagery but covering a considerably larger portion of the spill. For that reason, three visible and one near-IR band that best matched wavelengths used on the DMSC were chosen for processing, as listed in Table 1. Since WV-2 lacks a thermal IR band, which is utilized in OI's oil thickness algorithm, OI's algorithm could not be applied to the satellite data directly. Instead, the WV-2 4-band data set was run through a 200 class unsupervised (ISODATA clustering) classification with ERDAS software (using all 8 bands), and the resulting classes were then progressively merged to best match classification results obtained from near-time-coincident image sections covered by the DMSC/IR sensor inside the WV-2 footprint using the bands listed in Table 1.

An image set acquired on 21 May 2010 by the French Spot-5 satellite at 10 m resolution encompassed 3485 km² of the overall spill footprint. It was classified for oil thickness characterization using the same procedure as the WV-2 data and bands listed in Table 1.

2.5. TM satellite data processing and calibration

Multispectral imagery from the Thematic Mapper (TM) aboard Landsat-5 and Enhanced Thematic Mapper (eTM) aboard Landsat-7 satellites provided the most extensive spatial coverage of the DWH spill at a relatively high resolution of 30 m. Reasonably cloud-free imagery was available on 5/9, 5/10, 5/17, 6/10, 6/26, 7/4, 7/12 and 7/20/2010. The coverage was insufficient to completely contain the entire spill slick (as determined from SAR data) on any given day (it tended to miss the southeastern-most portion of the slick), however, since it contained the spill source site and large extents in all directions from it, the TM/eTM data likely contain the majority of areas covered with thicker-than-sheen oil accumulations. Aerial survey reports indicate that portions of the oil slick east of the TM/eTM coverage most often contained primarily sheens.

Our objective in utilizing the TM/eTM imagery was to further scale-up the aerial, WV-2 and SPOT high-resolution coverage of the DWH spill to obtain a more comprehensive understanding of the existing oil thickness patterns and distributions as they evolved through time. Hence, the initial idea was to apply multispectral classification methods using

near-time-coincident DMSC aerial image analyses for calibration/validation as was done with the WV-2 and Spot-5 data sets. We found, however, that despite their characteristically very high reflectance in the near-IR bands, oil emulsion features were usually not separable in the TM/eTM imagery. As is discussed in detail below, this was found to be due to their narrow shape which caused them to become subpixel features in most instances. This caused, in turn, their unique reflectance to be subdued by the dominant reflectance profile from the rest of each 30 m pixel. Oil emulsion features could only be directly isolated in cases where both their length and width exceeded the dimension of at least 1.5 or 2 TM/eTM pixels. An example is shown in Fig. 9. Likewise, we found that silver and rainbow sheen could not be reliably classified in the TM/eTM data because their increased reflectance in the short wavelength bands was insufficient to rise above the instruments' signal-to-noise limits.

Fig. 3 shows a multispectral rendering of the 9 May 2010 TM image, and corresponding DMSC/IR thermal image and oil classification zoom-ins over various parts of the slick covered by OI's imaging mission done within 2 h of the actual Landsat-5 orbit time. Analysis of aerial photos and DMSC/IR imagery from days that TM/eTM data are available revealed that, unlike with the WV-2 and Spot-5 data, which allowed classification of the oil film features directly, the multispectral reflectance profile of the TM/eTM pixels is a combined function of the type (i.e. thickness and emulsification extent) of oil features contained within, as well as how much of the sea surface was actually covered by them within each pixel. For example, a pixel with 30% of its area covered by an oil film in the metallic thickness range and the rest covered by sheen has a significantly different reflectance profile than a pixel with 60% “metallic” thickness coverage (as determined from near-time-coincident DMSC/IR data). A TM/eTM-based multispectral oil spill classification is thus not simply a depiction of oil thickness patterns but rather a characterization of both the spatial composition and density of the thicker oil features existing within each 30 m pixel.

For that reason, we chose to classify the TM/eTM imagery into the following simplified, basic classes describing the overall volume of oil within each pixel (rather than a non-sensical “average thickness”), using near-time-coincident DMSC/IR analyses for calibration and validation on days they were available. The zoom-ins in Fig. 3 serve as examples of the class-distinguishing characteristics in the DMSC/IR data:

Sheen: Areas contained in the TM/eTM coverage that are contained within the near-time-coincident SAR-determined oil slick footprint but show no significantly different reflectance profile from water areas outside the slick in the TM/eTM imagery.

Low Surface Oil Volume: Increased reflectance profile exists in multispectral TM/eTM data corresponding to thicker-than-sheen features revealed in DMSC data, but showing no features with thermal contrast in DMSC/IR imagery.

Mid-Volume: DMSC/IR imagery shows the corresponding TM/eTM area contains either (or both) unemulsified and emulsified oil features covering <20% of the TM/eTM pixel area. Oil features show a negative thermal contrast in DMSC/IR imagery. TM/eTM data show elevated reflectances in red and near-IR bands.

High Volume: DMSC/IR imagery shows the corresponding TM/eTM area contains both unemulsified and emulsified oil features covering >20% of the TM/eTM pixel area. Oil features show both negative and positive thermal contrast in DMSC/IR imagery. TM/eTM reflectance in red and near-IR bands is significantly higher than for the mid-volume class.

Very High Volume: Very large emulsion accumulations exhibiting high values in TM Band 7 – Band 1 difference and extensive positive thermal contrast in DMSC/IR aerial imagery of the same area.

The actual classification was accomplished in a procedure similar to that used for the WV-2 and Spot-5 data sets: a 200 class product was generated using ERDAS' ISODATA clustering algorithm, and these were then progressively reduced to fit the above final class criteria using the available DMSC/IR imagery for “calibration”. Near-time-coincident

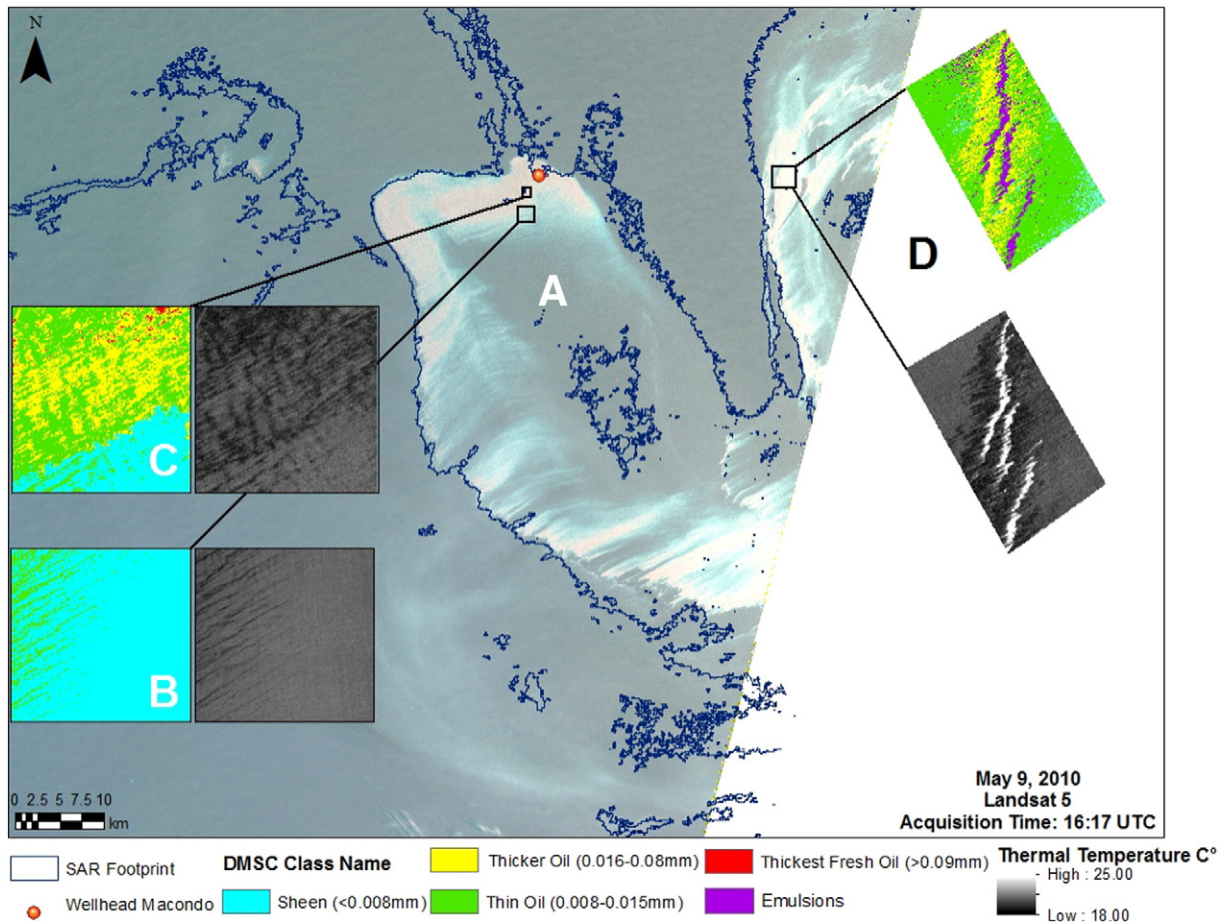


Fig. 3. Landsat-5 TM blue/green/near-IR rendition of portion of the DWH spill slick acquired on 9 May 2010. Insets show corresponding DMSC/IR oil thickness classification and thermal imagery examples in different parts of the TM-covered slick. The examples show characteristics corresponding to the different TM-derived oil volume quantification classes: (A) sheen, (B) low surface oil volume, (C) mid-volume, (D) high volume. The SAR-derived slick perimeter is also shown in the TM-covered portion.

DMSC/IR imagery was available for 5/9, 5/10, 7/4 and 7/20/2010. For days 5/17, 6/10, 6/26 and 7/12/2010 when DMSC/IR imagery was unavailable to use directly, average class cutoff values from the previous and post TM/eTM data sets were applied. The resulting classifications were further validated by utilizing available geolocated aerial photographs in NOAA's ERMA data base. Fig. 4 shows a representative TM data set and final classification.

3. Results

3.1. Dominant oil pattern distribution near the spill source region

The region encompassing a radius of roughly 20–30 km surrounding the MC-252 well site where fresh oil was upwelling was the most commonly imaged target area with OI's DMSC aerial sensor. At the request of multiple groups involved in the response, the region was imaged near-daily and sometimes twice-daily. DMSC imagery was thus the most frequent source of data for characterization of surface oil features present in the spill source region. The image classifications tended to show a distinct fresh oil plume which often assumed a triangular shape, with its origin above or up to a few hundred meters down-current from the well's position, and expanding progressively down-current for tens of kilometers, commonly past the boundaries of the imaged area (see Fig. 5). The plume's direction varied from day to day (presumably due to surface current and wind shifts), and on several occasions exhibited a prolonged, sustained rotation trend – such as during

5/20–26/2010 when daily imaging documented the plume's steady cyclonic rotation from an initial 5° bearing to 227° on 5/26/2010.

DMSC-derived oil thickness classifications of the fresh oil plume show it to contain a broad range of thicknesses encompassing all the fresh oil classes used in the DMSC-derived thickness products. As can be expected, the thickest classes tended to be found closest to the source location, with thinner films dominating further away as the oil naturally spread across the surface. Throughout the spill timeline, the DMSC data also sometimes show emulsified oil within the 20–30 km region around the well site. The emulsions were generally located outside the fresh oil plume and tended to have the form of elongated strands a few meters wide and up to 100+ meters long. Since emulsions tend to require considerable time to form, it can be assumed that the features represent aged, weathered oil that had been advected back to the immediate area around the source. Sea surface areas not occupied by the fresh oil plume and emulsion strands were covered with thin oil films ranging from very thin sheens (not directly detected with the DMSC but detected in same-day SAR imagery) to silver and rainbow-colored films (i.e. 0.04 to $5.0 \mu\text{m}$ (Bonn Agreement, 2007)).

As determined from the DMSC and SAR oil classifications, the sea surface surrounding the spill source thus tended to contain a relatively continuous range of oil thickness features spanning from the thinnest sheens to $90 + \mu\text{m}$ optically opaque fresh oil, as well as oil emulsions. This is especially true for DMSC data sets obtained in early to mid-May. After mid-May, the DMSC oil thickness classifications tend to show significantly less area covered by the thickest fresh oil classes. This observation appears to directly correspond to the timeline of

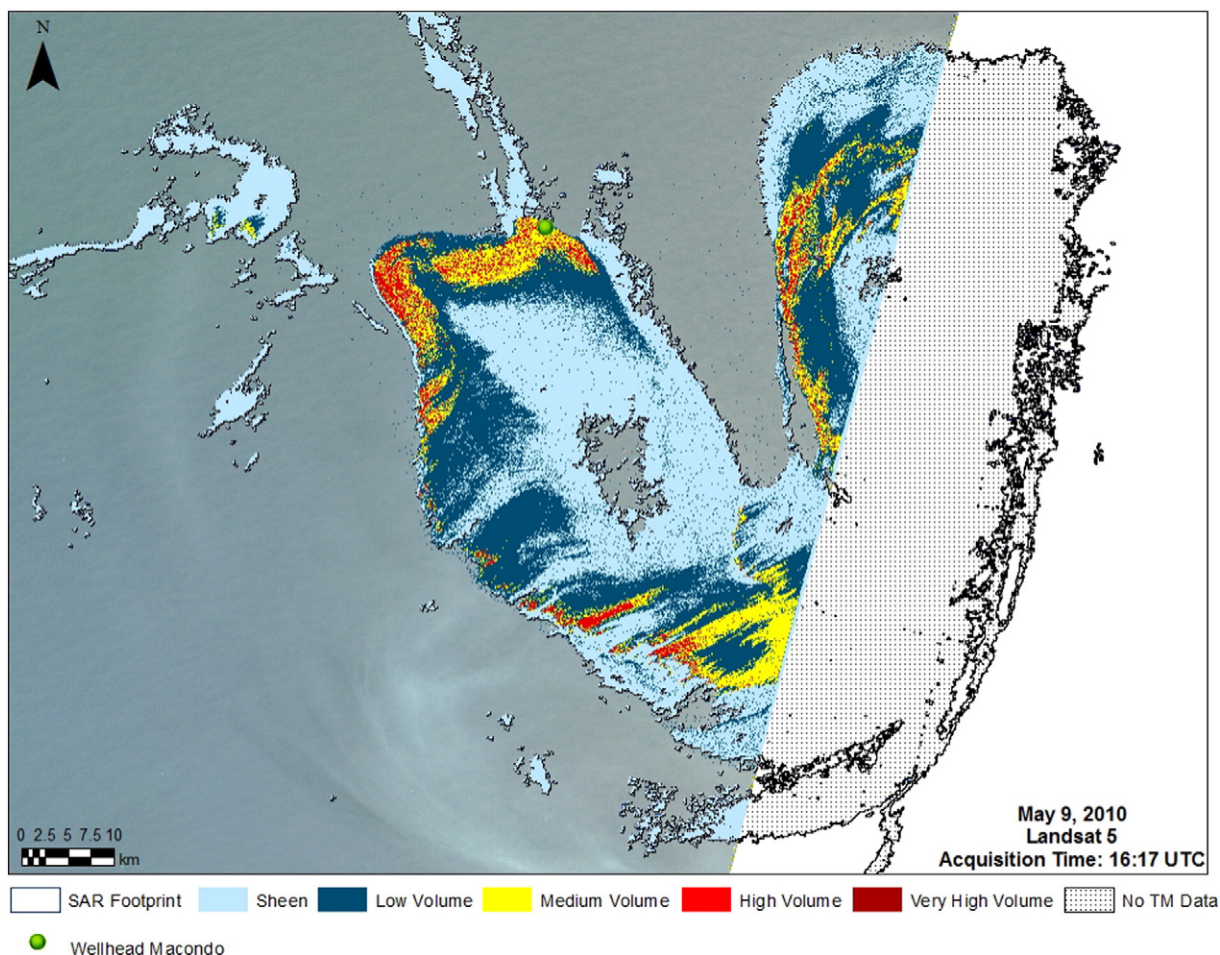


Fig. 4. Final TM-derived oiling characterization classification for 9 May 2010.

injections of dispersants into the well head at the bottom. The DWH oil spill was the first time this technique was attempted, its premise being that much smaller droplets would emanate from the jet of discharged oil, these small droplets would have much lower rise velocity to the point that at least a portion would remain entrained in the water column resulting in less oil reaching the sea surface.

Short-term tests of well-head dispersant injection using Corexit® 9500 were conducted in early May. OI's DMSC imaging was utilized during a 24 h test on 5/9–11/2010. Two imaging missions each day obtained multispectral/thermal imagery as well color photographs over the source area, all of which showed significant reductions in surfacing fresh oil volumes during the injection period. Although Corexit® 9500 was approved for use by the Environmental Protection Agency (EPA) prior to the spill, federal agencies did not allow operational use until 5/15/2010. The injection then continued uninterrupted, with the exception of a few multi-hour stoppages caused by well-control operations or equipment failure, until stopped a few hours before the well was capped on 7/15/2010.

Fig. 6 shows the relationship between the daily subsurface injection volume of Corexit® 9500 and the surface area fraction covered by the DMSC-derived two thickest fresh oil classes (i.e. fresh oil films thicker than 16 μm) within a 7 km radius centered on the well head. (The large image data gap from late June through mid-July is due first to the grounding of the aircraft during the passage of tropical storm Alex, and then to a switch in mission imaging priorities to inshore areas.) The data clearly show the reduction in thick oil coverage during the 5/9–11/2010 test, and the sustained increase in thick oil coverage during the subsequent injection shutdown. Following injection resumption, on days when imagery was available, the data show marked reductions

in areas with thick surface oil around the well head, especially on days when the injection volume was above approximately 10,000 gal. The only exceptions are 5/6/2010 and 5/7/2010 when no dispersant was injected but only <8% of surface area within the 7 km radius was covered by thick oil. This was due to the fresh oil plume's being advected from the well region in an anomalously long and narrow stream, as can be seen in the 5/6/2010.

DMSC imagery and oil thickness analysis shown in Fig. 2. Such a fresh oil plume dispersal pattern was never observed again. A thick oil area spike on 7/15/2010 corresponds to the stoppage of subsea dispersant injection for a few hours prior to the final well capping. Our data thus document a significant effect of the subsea dispersant injections on the oil film thickness distribution around the spill source site. The DMSC-derived observations are further supported by analysis of color photographs taken on the same flights, which tend to show dark, optically opaque portions of the fresh oil plume on days that small or no dispersant injections occurred and much lighter-colored, transparent oil film signatures dominating the plume on later days when dispersant injections were > 10,000 gal per day. Examples are shown in Fig. 5.

3.2. Oil distribution patterns outside the spill source region

For this study, high resolution (≤ 5 m) multispectral imagery from areas of the spill outside the approximately 30 km radius source region is available from OI's DMSC aerial sensor on multiple days throughout the event, as well as from the WV-2 satellite image set acquired on 6/15/2010, and Spot-5 satellite image set acquired on 5/21/2010.

In areas that contained significant amounts of thicker-than sheen oil features, oil thickness classifications from all 3 data sources show very

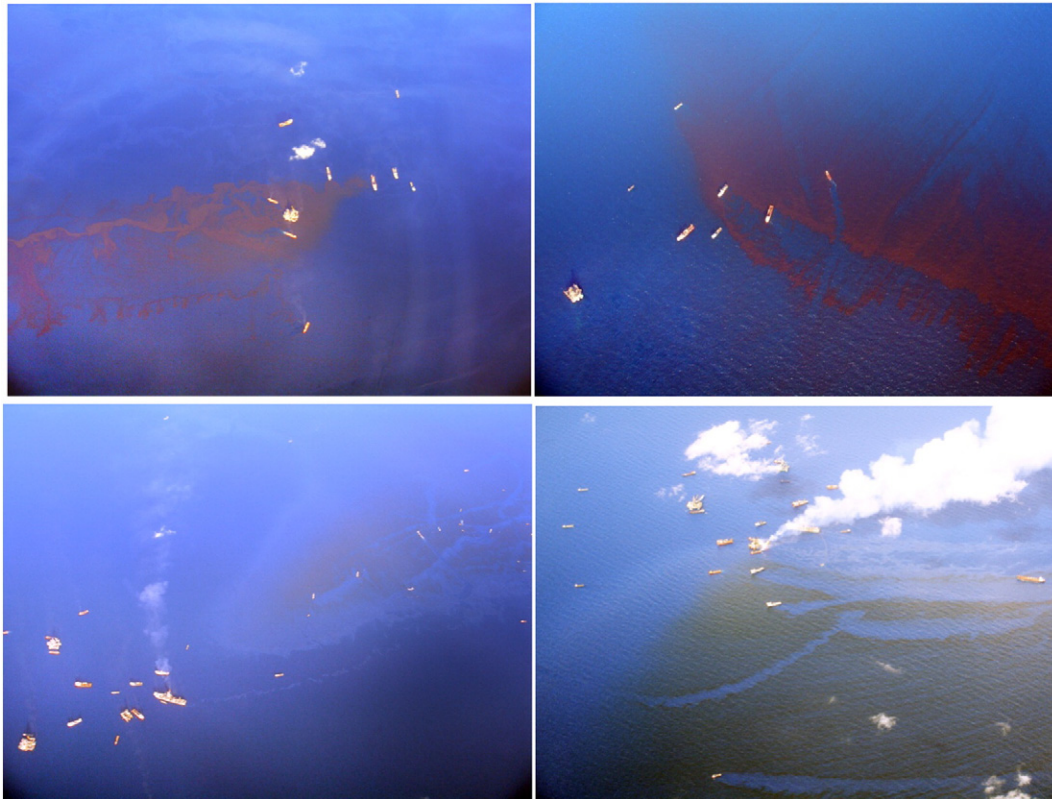


Fig. 5. High altitude aerial photos of the MC-252 well site showing examples of the freshly upwelled surface oil plume. On 5/6/2010 (top left) and 5/13/2010 (top right) no subsurface dispersant was being injected at the well head and the plume above it primarily consisted of relatively thick, optically opaque oil. Images from 5/23/2010 (bottom left) and 7/4/2010 (bottom right) show the plume during high-volume subsurface dispersant injections. Unlike before the injections began, the plume is primarily composed of thinner, translucent oil films.

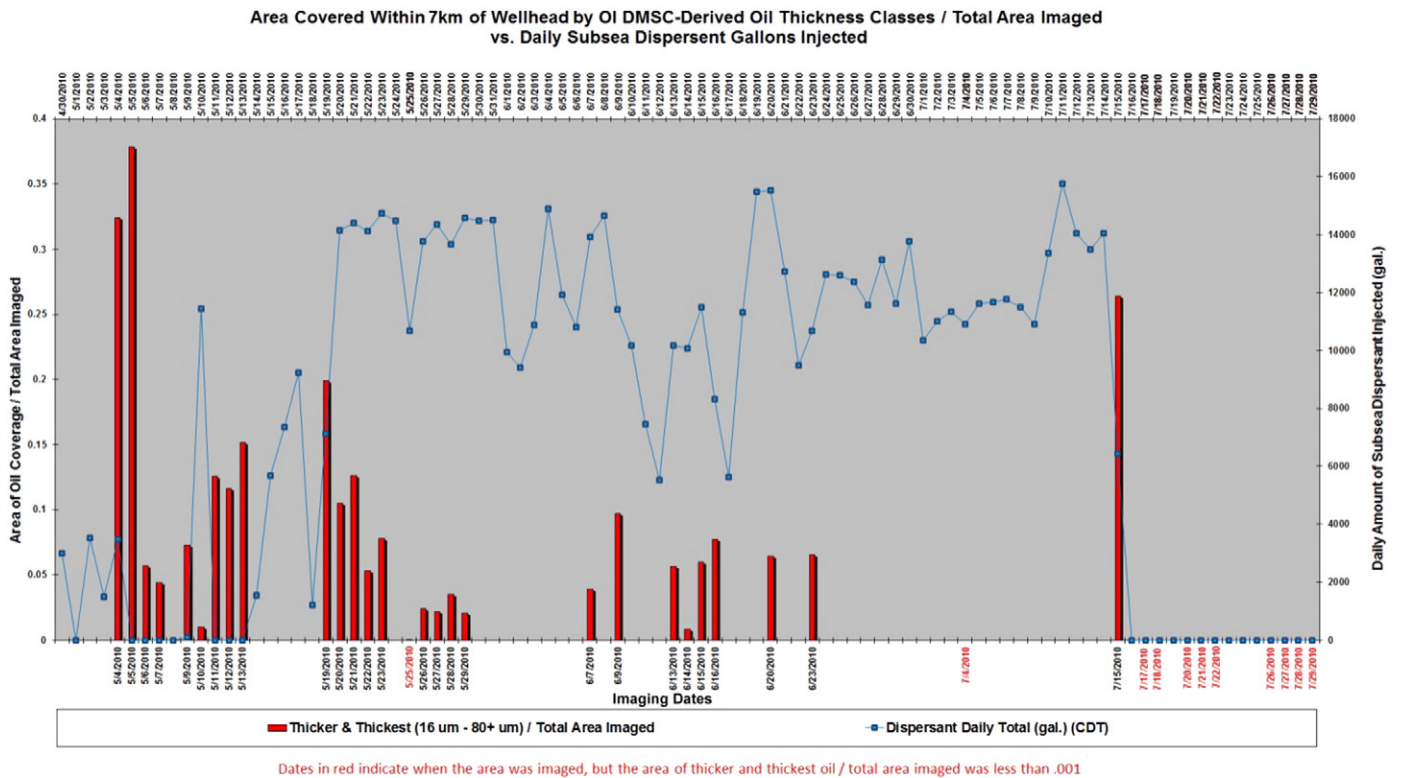


Fig. 6. Total surface area fraction within a 7 km radius centered on the MC-252 well location that was covered by DMSC-derived fresh oil thickness > 16 μm on days the source site region was imaged (red) vs. volume of Corexit® 9500 released at the well head during each 24 h period (blue). Dates in red indicate days when imaging was done but no oil film thicker than 16 μm was detected within the 7 km radius. No source site imagery was available on dates not listed on the bottom.

similar oil feature characterization results: Unlike within the spill source region where a relatively continuous progression of oil thicknesses usually existed, sampled regions further away tended to contain only a few oil characterization classes with very distinct spectral/thermal characteristics and a discontinuous oil layer thickness progression. Specifically, in areas that contained oil films thicker than the very thin sheens detectable only in SAR data, oil features can be grouped into 3 thickness characterization classes: 1) extensive areas of silver sheen and rainbow-reflecting film (i.e. 0.04 to 5.0 μm); 2) large areas of film with visible-nearIR reflectance and thermal-IR emittance characteristics of Bonn Agreement's "metallic" Code 3, and OI's own experimental results (Svejkovsky and Muskat, 2009) corresponding to a range of approximately 6–70 μm ; and 3) oil emulsions, most commonly in the form of strands up to several hundred meters long and usually <50 m wide. From ship-based field sampling done during the spill (Belore et al., 2011), the emulsions varied in thickness from a few millimeters to occasionally as much as a few centimeters. Consistently lacking in spill areas outside the source region were features consisting of unemulsified oil layers with visible-nearIR reflectance and thermal emission characteristics corresponding to thicknesses greater than approximately 70 μm . As was discussed in Section 2.1 above, such crude oil films have multiple unique reflectance and emission characteristics that make them readily distinguishable from thinner oil films and emulsions.

The 3-class oil feature characterizations were found to persist both in space and in time. Especially useful for this analysis were data from OI's DMSC/IR aerial sensor acquired on 5/10/2010, Spot satellite imagery from 5/21/2010, and WV-2 satellite imagery from 6/15/2010. The

DMSC imaging flight obtained swaths of image data in a star-shaped pattern within the entire spill footprint (as determined from SAR-sensed slick signatures) thus methodically sampling different sections of the spill (see Fig. 1). The Spot-5 and WV-2 data sets represent the largest contiguously sampled areas at sub-10 m resolution (323 km² and 3485 km², respectively). The three data sets thus provide a relatively large-scale but very high resolution view of oil features existing on 3 separate days within the spill footprint, spanning more than a month-long time interval.

The oil emulsion features differed markedly in shape from the thick sheen and metallic thickness features. They were consistently elongated and narrow with sharply defined edges, resulting in a consistently high length-to-width ratio. Generally, the only locations where the emulsion features were wider than approximately 30–50 m were areas where two or more of the strands had intersected, collided and locally merged. In contrast, the thick sheen and metallic thickness features tended to be more spread out in both directions with complex, undulating edges, and often interconnected with each other at one or more locations. Examples in Fig. 7 show the shape characteristics of the 3 oil feature types. To quantify the spatial and temporal consistency of the distinctly shaped emulsion features, the length-to-width ratios were manually measured for a representative sample of each oil characterization class using polygons obtained from the classification product of DMSC data acquired throughout the slick on 5/10/2010, Spot-5 data from 5/21/2010 and WV-2 data from 6/15/2010. The results are presented in Table 2. In measuring the "length" and "width" of a polygon we strived to capture two representative measurements in perpendicular

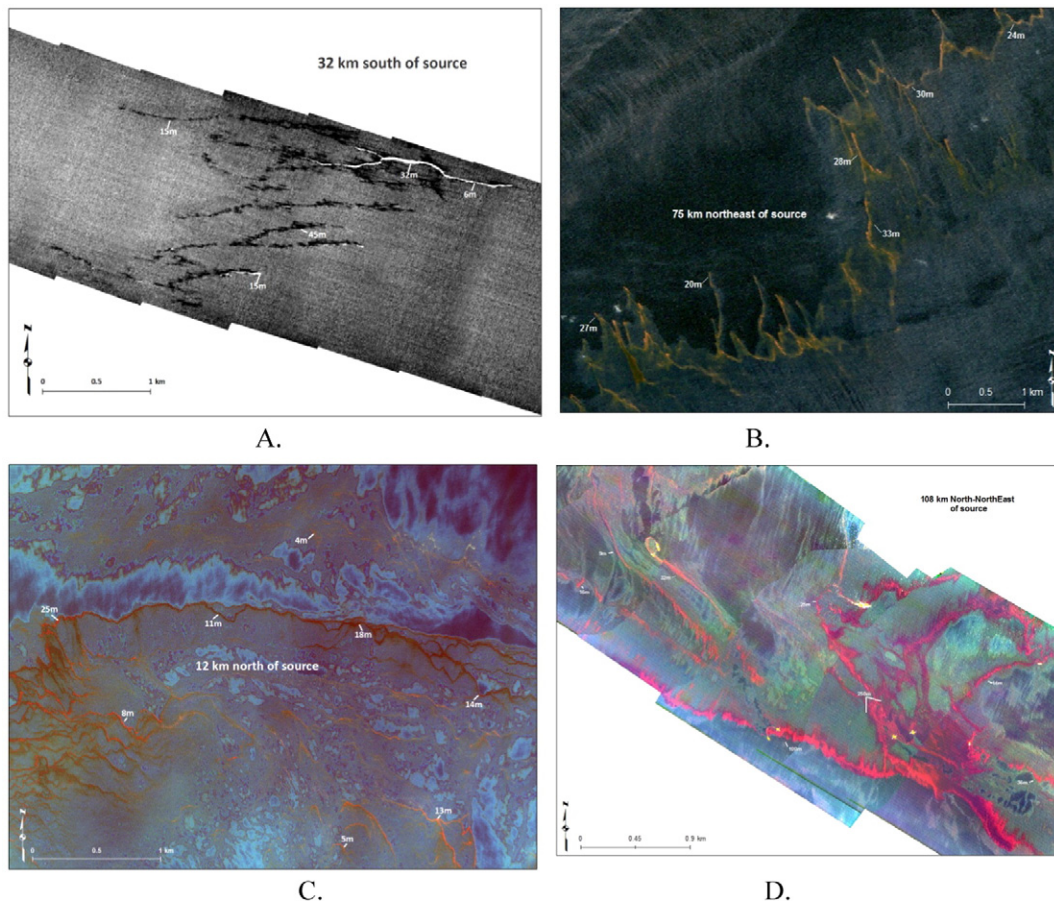


Fig. 7. Sample images of sheen, metallic and emulsion oil features existing in regions away from the spill source site, also showing representative widths of the emulsion strands: (A) Thermal IR rendition from the DMSC/IR sensor on 5/10/2010 (note that the sheen and metallic thickness features exhibit no thermal contrast signal and hence are not visible); (B) blue/green/near-IR band rendition from a SPOT-5 image on 5/21/2010; (C) blue/green/near-IR rendition from WV-2 image on 6/15/2010 showing emulsion strands amid large areas of metallic films and sheens; (D) blue/green/near-IR rendition of DMSC/IR data on 6/21/2010 showing several of the strands merging into a very wide feature.

Table 2
Feature shape statistics from the three very high resolution sensors of sample emulsion strands located throughout each data set.

Sensor	Acquisition date	Number of samples	Average length:width ratio	Standard deviation length:width ratio
DMSC/IR	5/10/2010	45	8.26	6.49
SPOT	5/21/2010	49	5.14	4.44
WV-2	6/15/2010	61	6.35	4.19

orientations. It is important to note that in many instances multiple individual emulsion strand features remained oriented in-line with each other, thus extending on occasion the strand-like nature of the regional emulsion aggregations for hundreds of kilometers. Obviously, such an approach is not entirely objective, however, applying fully automated methods such as computation of the Shoreline Development Ratio index which relates a polygon's area to its boundary length (Hutchinson, 1957) could not be used due to the extreme spatial complexity of the edge of most thick sheen and metallic polygons, which greatly increases its computed boundary length.

Even taking its limitations into account, the analysis provides two important results for floating oil features outside the spill source region: 1) The oil was distributed in features having only a limited number of thickness ranges and specific spatial structure; 2) these characteristics were already in-place through much of the slick area on 5/10/2010 (i.e. 20 days after the spill began) and quite possibly earlier, and remained consistent throughout the spill duration.

It should be noted that the passage of tropical storm Alex over the spill area during the last 2 days of June 2010 had a very extensive effect on reducing the amount of floating oil. OI flew its first post-storm mission on 7/3/2010 and noted both visually and through its DMSC image analysis a major disappearance of oil features along the flight path between the source and the Alabama coast. This included both sheen areas and thicker oil features. The storm effect was also noted during analysis of coarser resolution but significantly larger coverage area data from the TM satellite sensors, as is described in the next section.

3.3. Oil distribution characterization with Landsat TM satellite sensors

The major potential advantage of upscaling the multispectral oil characterization algorithms from the high resolution aerial and satellite sensors to the 30 m resolution TM imagery is the TM's much larger spatial coverage. Throughout the DWH event TM data from Landsat-5 and Landsat-7 covered 50–80% of the entire spill footprint (based on SAR imagery which covered the entire slick). As was already mentioned in Section 2.5, however, a somewhat surprising initial finding was that in most cases, despite their uniquely high red and near-IR reflectance, emulsified oil features are not commonly directly detectable in TM multispectral data. We believe this is due to the size the emulsion features usually attain versus the TM's 30 m pixel resolution, coupled with only 8-bit dynamic range and relatively low signal-to-noise ratio. As is discussed above, based on analysis of aerial and satellite imagery with resolutions better than 6 m, the majority of emulsified oil features in the DWH spill footprint commonly had a width of 30 m or less, i.e. they were sub-pixel elements (in one direction) in the TM imagery. Further evidence was provided by direct comparisons of emulsion features identified in OI's DMSC/IR sensor imagery acquired within hours of the satellite overpasses on 5/9, 5/10, 7/4 and 7/20/2010.

As is also noted in Section 2.5, some TM and eTM images contain elongated features 2–5 pixels wide that exhibit uniquely elevated reflectances in the instruments' red, near-IR and shortwave-IR bands. Comparisons with near-time-coincident geolocated aerial photos (and on 5/17/2010 with high resolution imagery from NASA's Airborne Visible/Infrared Imaging Sensor) show that these features correspond to unusually wide accumulations of oil emulsions. Examples are shown in Fig. 8. TM's and eTM's ability to detect oil large emulsion features appears to be inconsistent both temporally and spatially (i.e. within different portions of each image), however, even if they are large enough to

saturate multiple pixels. It is possible that view angle and atmospheric attenuation factors reduce the signal-to-noise ratio to levels below the detection threshold. For example, the features resolved in the 5/10/2010 Landsat 7 image are not detectable in a Landsat 5 image acquired the preceding day (in fact, the TM 5/9/2010 image shows no such features anywhere in the spill). It is unlikely that all of the very large emulsion accumulations would have formed overnight, so at least some should have been detectable in the 5/9/2010 image. TM's and eTM's ability to detect strands of very heavy oil emulsions is challenged just as it is with high resolution SAR imagery (although based on different physical principles) where the success strongly depends on incidence angle, sea state, etc. (Garcia-Pineda et al., 2013b).

The much wider spatial coverage provided by the TM imagery allows a more comprehensive assessment of oil feature distributions within the DWH spill footprint through time. When classified for floating oil concentrations as described in Section 2.5 above, and combined with the overall oil slick footprint from same-day SAR data, it is possible to assess the locations and surface area covered by high and low density accumulations of oil features thicker than sheens on days when Landsat data are available. Table 3 lists surface area values of each oil concentration class for all TM data sets used in this study. It is important to note that since each TM image failed to cover the southeastern portion of the slick footprint, the coverage values represent each class' coverage only within the TM-imaged area, not the entire spill footprint. The SAR-derived "thin sheen" coverage was also computed only from the TM-imaged area. However, as has already been mentioned, based on OI's and other aerial observers' overflights, the far southeast portion of the slick tended to contain mostly sheens and not the same densities and frequencies of heavier oil accumulations observed by the TM-covered regions through most of the event.

The available data show that throughout the spill event, surface coverage within the overall slick footprint was dominated by sheen-thickness films. Large areas containing low and high concentrations of metallic thickness areas and oil emulsion strands tended to primarily remain offshore, however by mid-May and into June as the overall slick footprint expanded, some concentrated areas drifted northeastward toward the mainland. Some accumulations also drifted westward and northwestward, ultimately affecting areas in and around the Mississippi Delta, which was not included in this study. As was already noted, the passage of tropical storm Alex over the spill during the last two days of June caused a dramatic reduction in surface oil features. This is clearly reflected in the Table 3 data: through May and June the sea surface area covered by the non-sheen oil concentrations generally increased, culminating in highest-ever values for the low, high and very-high classes in the 6/26/2010 TM5 data set. This also corresponds to the largest overall SAR-sensed oil slick footprint within the TM's coverage area. The next available TM data set on 7/4/2010 (i.e. 4 days after the storm's passage) shows a dramatic decrease in coverage areas by all oil characterization classes, as well as an 85% decrease in overall SAR-sensed slick footprint. The 7/12/2010 classifications indicate that the overall surface oiling reduction persisted through July until the well was permanently capped three days later.

It is important to note that the combined SAR/TM analysis reveals that most of the overall slick footprint consisted of primarily sheen. This is quantified in Table 4 which shows the proportion of the overall slick within TM's coverage that contained thicker-than-sheen oil accumulations at sufficient surface densities to be detected by the TM analysis. Such coverage remained below 50% of the imaged

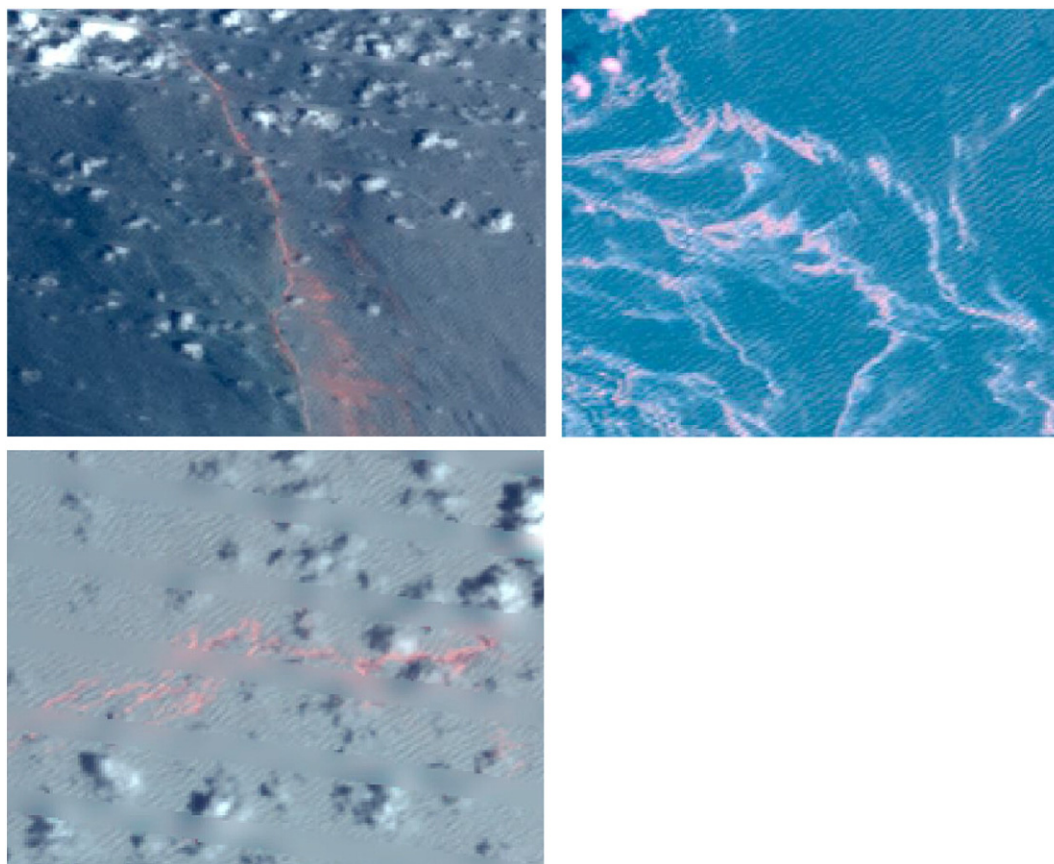


Fig. 8. eTM blue/green/near-IR images from Landsat-7 acquired on 5/17/2010 (left upper and lower) and TM image from Landsat-5 acquired on 6/26/2010 (above) showing elongated red features corresponding to abnormally wide aggregations of thick oil emulsions.

slick area throughout the event and actually decreased significantly from May through June, while the overall (SAR-sensed) footprint increased. (As was already mentioned, the TM's geographical coverage excluded the southeastern portion of the full slick footprint, which, based on aerial surveys, tended to have the least accumulations of heavy oil targets. Hence it is likely that the fraction of thicker-than-sheen oil areas within the full slick would have been even lower if the entire spill footprint could be sampled.) This suggests that the sizeable increase in the overall spill footprint into June was driven by expansions of areas covered primarily by oil sheen. Wind strength (and related vertical turbulence and increased evaporation rates) is an important factor affecting thin sheens. Low wind conditions favor the preservation of sheens. Our data reflect this – the doubling

of sheen area on 6/26/2010 from earlier data days corresponds to wind speeds below 16 km per hour during the prior 48 h. Conversely, our results show that the thicker-than-sheen area fraction doubled in the 7/4/2010 TM data – i.e. four days after the passage of tropical storm Alex. This seems logical, since the heaviest oil accumulations likely resisted the storm's turbulence effects the most, while the sheen films succumbed to the effects of high winds, rain and vertical mixing.

4. Discussion

Our study revealed several characteristics of crude oil behavior during a large, continuous offshore spill that have not been previously

Table 3

TM-derived oil classifications vs. total SAR-derived oil slick area covered by each TM scene. The TM areas do not include cloud-contaminated pixels or data lines missing in eTM imagery.

Date	TM sensor	SAR-derived oil area (km ²) ^a		TM-derived oil area (km ²) ^a			
		Thin sheen		Low-volume	Mid-volume	High-volume	Very high-volume
5/9/2010	TM5	1502.87		903.91	242.67	101.26	0.00
5/10/2010	TM7	1940.03		1073.71	446.49	127.91	0.00
5/17/2010	TM7	6025.69		2149.17	940.70	155.32	2.72
6/10/2010 ^b	TM5	6964.42		1789.95	738.26	5.63	0.18
6/10/2010 ^c	TM5	5763.56		1789.95	738.26	5.63	0.18
6/26/2010	TM5	10,404.12		2428.56	522.09	156.12	3.34
7/4/2010	TM7	1506.79		731.19	250.25	81.42	0.00
7/12/2010	TM5	1672.71		441.00	217.48	30.76	0.58
7/27/2010	TM7	7787.35		113.33	24.56	2.45	0.00

^a Excludes drop-out lines, clouds, artifacts.

^b SAR acquisition time was 36 h and 58 min *earlier* than TM acquisition time.

^c SAR acquisition time was 30 h and 21 min *after* the TM acquisition time.

Table 4
Area percentage of TM-derived thicker-than-sheen oil concentrations vs. SAR-derived oil slick area covered by sheen. The TM areas do not include cloud-contaminated pixels or data lines missing in eTM imagery.

Date	SAR identifier	TM sensor	Acquisition time (UTC):		Area (km ²) ^a within TM footprint of:			Percent of total area covered by:		
			SAR	TM	SAR-derived surface oil	TM-derived thicker-than-sheen oil	SAR-derived thicker-than-sheen	TM-derived thicker-than-sheen oil		
5/9/2010	050910 155007	TM5	15:50:07	16:17:00	2750.71	1247.84	54.6%	45.4%		
5/10/2010	051010 114822	TM7	11:48:22	16:18:00	3588.14	1648.11	54.1%	45.9%		
5/10/2010	051010 235314	TM7	23:53:14	16:18:00	5172.10	1648.11	68.1%	31.9%		
5/17/2010	051710 114506	TM7	11:45:06	16:18:00	9273.60	3247.91	65.0%	35.0%		
6/10/2010	060910 035621	TM5	03:56:21 ^b	16:17:00	9498.45	2534.02	73.3%	26.7%		
6/10/2010	061110 233901	TM5	23:39:01 ^c	16:17:00	8297.59	2534.02	69.5%	30.5%		
6/26/2010	062610 162543	TM5	16:25:43	16:17:00	13,514.22	3110.10	77.0%	23.0%		
7/4/2010	070410 234751	TM7	23:47:51	16:18:00	2569.65	1062.86	58.6%	41.4%		
7/12/2010	071210 235323	TM5	23:53:23	16:17:00	2362.54	689.83	70.8%	29.2%		
7/20/2010	072010 003818	TM7	0:38:18	16:18:00	7927.68	140.34	98.2%	1.8%		

^a Excludes drop-out lines, clouds, artifacts.

^b SAR acquisition time was 36 h and 58 min earlier than TM acquisition time.

^c SAR acquisition time was 30 h and 21 min after the TM acquisition time.

documented: 1) specific oil film thickness and weathering characteristics that persisted both in time and space throughout the 3-month event; 2) the effectiveness of subsurface dispersant injections at the well head to reduce the amount of oil reaching the surface; 3) the overall composition of the surface oil slick through time with respect to sheen vs. thicker oil accumulations and the effect of a tropical storm event; 4) the importance of image resolution for correctly locating areas with actionable oil targets and quantifying their accumulation densities.

Our analysis revealed that a fairly continuous progression of oil film thicknesses existed in the vicinity of the MC-252 well head where fresh oil continuously upwelled. In the early part of May when subsurface dispersants were not yet in-use, some of the thickest fresh oil over the well head exhibited positive thermal contrast of up to 4 + °C relative to surrounding water/sheen areas in OI's DMSC aerial imager. This indicates the oil existed, at least for some time, in thicknesses exceeding 200 µm (Svejkský and Muskat, 2009). During the subsurface dispersant injection tests and following a sustained ramp-up in daily injection rates above 10,000 gal per day on 5/20/2010, analysis of OI's aerial multispectral imagery shows a marked decrease in areas covered by thick fresh oil around the well. We believe this was a direct consequence of the dispersant injections. The variations in thick oil coverage that correspond closely to variations in injected dispersant volumes before, during and after the tests, the subsequent multi-day shut-down, operational increase on 5/20/2010, and stoppage of injection on 7/15/2010 support the contention that dispersant injection was indeed the dominant causative factor rather than just a marginal augmentation to natural dispersion during rise of the oil through the deep water column as some had suggested (Peterson et al., 2012; Aman et al., 2015).

Outside of the spill source region our analysis found that the oil features exhibited a somewhat simplified, discontinuous thickness characterization structure. Areas containing floating oil features thicker than sheen and rainbow-appearing films tended to be covered by translucent films in the 6–70 µm range (encompassing and slightly exceeding the Bonn Agreement's "Code 3 – metallic" range). Markedly lacking were areas covered by a homogenous film of thicker oil. Our finding concurs with observations made during annual "Oil on Water" exercises done off Europe during which freshly spilled oil also assumes in time similar thickness characteristics (J. H. S. Andersen, pers. commun.). This may be due to several reasons: first, crude oils (especially relatively light ones such as was present in the MC-252 well) tend to spread out quickly on an unbounded water surface, initially due to buoyancy-inertia forces and ultimately to viscosity and surface tension (Fay, 1971). The more time and hence distance the oil had been on the surface since its upwelling from the well, the thinner it is expected to get, aided by dispersion through winds, waves and currents. Second, it is widely recognized that up to 30% of the spilled oil's original volume evaporated within the initial 24 h (Lehr et al., 2010) as its most volatile components escape. This not only reduces the oil film's thickness but also changes its composition. Such continued concentration of the crude's heavier components through weathering can be expected to ultimately lead to a stable "terminal thickness range". In contrast, refined light petroleum products such as gasoline, jet fuel and diesel that lack the heavier components tend to spread out to sheen-type thicknesses in an unbounded environment and ultimately evaporate into the air or dissolve and disperse into the water. We suspect the "terminal thickness range" is specific to the crude oil type and may be different for markedly heavier oils. For example, OI's analysis of DMSC data acquired over the *M/V Cosco Busan* spill in San Francisco Bay in 2007 showed a discontinuous oil feature thickness distribution spanning sheens-to-very thin films, patches of fresh oil > 200 µm, and oil emulsions. Lacking were oil targets with thicknesses between approximately 50 µm and 200 µm (Svejkský et al., 2008). The oil involved in that incident was IFO-380 bunker fuel – a vastly more viscous product.

The second type of dominant thicker-than-sheen/rainbow oil features in areas away from the DWH spill source site revealed by our

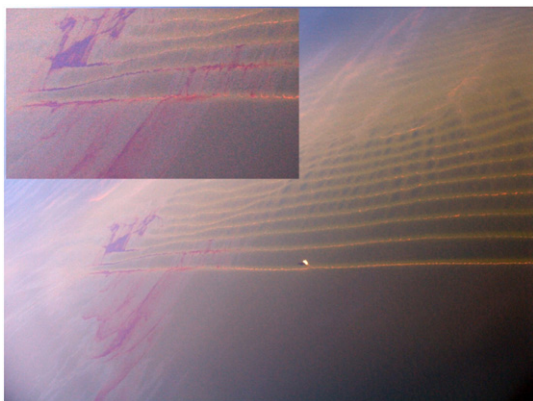


Fig. 9. Oblique photo of an extensive Langmuir circulation field acquired on an OI imaging flight on 6/13/2010. The yellow material is likely seaweed/biogenic material and the dark red-brown is weathered oil. The bright object in the middle is an oil rig. Inset shows the oil being formed into concentrated strands by the circulation.

analysis were elongated (sometimes 100 s of meters) but usually narrow (<30 m) strands of oil emulsions. Using OI's DMSC multispectral imagery, these features exhibited reflectance properties specific for emulsified oil, and a wide range of thermal emittance properties indicative of a broad range of thicknesses and oil/water ratios (Svejkovsky and Muskat, 2012B), in agreement with field sampling analyses done during the spill (Belore et al., 2011). As was the case with the “metallic” range oil film areas, these features exhibited persistent shape characteristics both spatially and temporally throughout the event.

The relative consistency of the emulsion features' distinct elongated, narrow shape both in space and time invites speculation on their formation mechanism. Analogous to the formation of weed-lines and strands of accumulated biogenic materials that were commonly observed over the Gulf of Mexico during the spill, an obvious suggestion is the accumulation of weathered, viscous oil along current shear and convergence zones. A variation of this that was observed by OI multiple times during

the imaging flights was the entrainment of oil in Langmuir circulation cells. An example is shown in Fig. 9. This process not only formed elongated strands of weathered oil but acted to further concentrate it. The linear aggregation effect of Langmuir circulation cells has also been observed previously with freshly discharged crude oil during open water field experiments off Europe (Rye, 2001).

As was already noted, the overall oil slick footprint was dominated by sheen, much of it too thin to adequately alter the sea surface reflectance to be detected in aerial and satellite multispectral imagery. Based on OI's DMSC overflights as well as analysis of the combined SAR/TM oil characterizations, some of these vast sheen areas existed hundreds of kilometers distant from the spill source site where the oil initially reached the surface. Since the floating oil was constantly subject to evaporation and degradation by UV radiation, biogenic factors, and mixing into the water column, it is questionable how a petroleum film a few microns thick could continue to exist for the days or weeks it would have taken for it to drift such distances. Based on analysis of our high resolution data, we posit the following explanation: visual observations during the OI flight missions backed by multispectral data processing from the DMSC aerial and WV-2 and Spot-5 sensors show that the large sheen regions routinely contained isolated, often relatively small emulsified oil features. These features tend to continue to release petroleum residue along their periphery, which spreads into a very thin sheen layer – thus continuously replenishing the overall sheen in the area. An example from the midst of a large thin sheen region 42 km south of the source site was imaged on 5/13/2010 with OI's DMSC sensor and is shown in Fig. 10. The data show three small emulsion features “bleeding off” silvery sheen around their perimeter. Visual survey notes from that flight indicate that in that region perhaps one such group existed per several square kilometers of ocean surface. Because of the spatial sparsity and small size, such features are not detectable in SAR, and in multispectral imagery with resolutions coarser than approximately 5–10 m. The generation of vast sheen areas by isolated patches of oil emulsions was actually observed during the DWH event, both experimentally and naturally in the field by Belore et al. (2011) under rough as well as calm sea conditions (they called the process “sheening”).

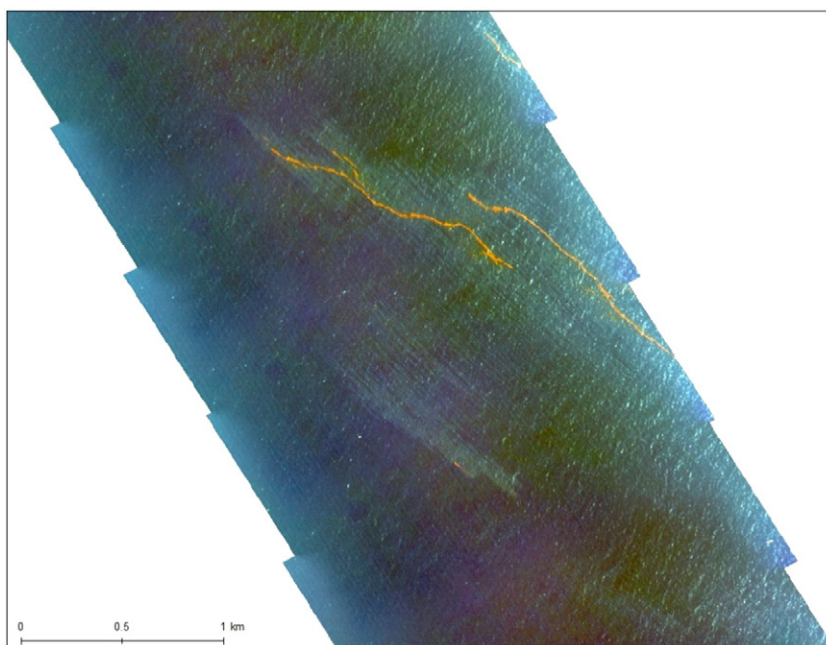


Fig. 10. DMSC multispectral (710/551/450 nm as RGB) image mosaic of small isolated oil emulsion features imaged within a vast sheen area 42 km south of the spill source on 5/13/2010. The light signatures around the emulsion strands are from silver sheen dispersing from the emulsions.

Our analysis indicates that very high resolution (≤ 10 m) aerial and satellite imagery are able to directly provide size and spatial extent information on individual oil features of the three non-thin-sheen characterization types. Coarser resolution data, including TM (27 m), do not provide such capability – particularly for the thick, emulsified oil distributions. Instead, their pixel reflectance characteristics are linked to the accumulation density of the three dominant oil characterization classes within each pixel. For that reason, such coarser resolution imagery provides limited utility for tactical, near-real-time applications during spill response, since it cannot be directly used to reliably locate actionable oil targets. On the other hand, during large oil spills, when calibrated as done in this study, the coarser imagery can provide a uniquely broad-area synoptic assessment of which portions of the entire spill footprint likely contain the heaviest oil accumulations. Such imagery can then be used to more efficiently allocate other remote sensing and on-water resources and, as was done here, conduct post-spill assessments on the role of natural and anthropogenic influences on the progression of the spill.

Acknowledgements

The initial data collection, processing and analysis done by Ocean Imaging Corp. during the DWH event was funded by BP America, with aircraft and pilot crew provided by NOAA. Analyses reported in this study were funded by NOAA through Stratos Consulting Inc., contract no. AB133C-11-CQ-0051. We thank DigitalGlobe Corp. for making the 6/15/2010 WV-2 imagery available to OI for research purposes. All Landsat imagery was obtained through public access at <http://earthexplorer.usgs.gov/>. Spot imagery was obtained from the US Geological Service under a research agreement.

References

- Alpers, W., Hühnerfuss, H., 1988. Radar signatures of oil films floating on the sea surface and the Marangoni effect. *J. Geophys. Res.* 93, 3642–3648.
- Aman, Z.M., Paris, C.B., May, E.F., Johns, M.L., Lindo-Atichati, D., 2015. High-pressure visual experimental studies of oil-in-water dispersion droplet size. *Chem. Eng. Sci.* 127, 392–400.
- Belore, R.C., 1982. A device for measuring oil slick thickness. *Spill Technology Newsletter* 7 (2), 44–47.
- Belore, R.C., Trudel, K., Morrison, J., 2011. Weathering, emulsification, and chemical dispersibility of Mississippi canyon 252 crude oil: field and laboratory studies. *Proceedings of the International Oil Spill Conference 2011*, 23–26 May, Portland, Oregon (unpaginated USB flash drive).
- Bonn Agreement, 2007. Bonn Agreement Aerial Surveillance Handbook, Version 25, October 2007, URL: <http://www.bonnagreement.org/eng/doc/Aerial%20Surveillance%20Handbook%202004%20-%20English%20version.pdf>, (96 pp.).
- Brekke, C., Solber, H., 2005. Oil spill detection by satellite remote sensing. *Remote Sens. Environ.* 95, 1–13.
- Byfield, V., 1998. Optical remote sensing of oil in the marine environment. U. of Southampton, School of Ocean and Earth Science (PhD Dissertation).
- Fay, J.A., 1971. Physical processes in the spread of oil on a water surface. *International Oil Spill Conference Proceedings: June 1971* 1971 (1), 463–467.
- Fingas, M.F., Brown, C.E., 2011. Oil spill remote sensing: a review. In: Fingas, M. (Ed.), *Oil Spill Science and Technology: Prevention, Response, and Clean Up*. Elsevier, Burlington, MA, pp. 111–169.
- Gade, M., Alpers, W., Hühnerfuss, H., Masuko, H., Kobayashi, T., 1998. Imaging of biogenic and anthropogenic ocean surface films by the multifrequency/multipolarization SIR-C/X-SAR. *J. Geophys. Res.* 103 (C9), 18,851–18,866.
- Garcia-Pineda, O., MacDonald, I.R., Li, X., Jackson, C.R., Pichel, W.G., 2013a. Oil spill mapping and measurement in the Gulf of Mexico with textural classifier neural network algorithm (TCNNA). *IEEE Journal of Selected Topics in Applied Earth Observations and Remote Sensing* 6 (6), 2517–2525.
- Garcia-Pineda, O., MacDonald, I., Hu, C., Svejkovsky, J., Hess, M., Dukhovskoy, D., Moorey, S., 2013b. Detection of floating oil anomalies from the Deepwater Horizon oil spill with synthetic aperture radar. *Oceanography* 26 (2), 124–137. <http://dx.doi.org/10.5670/oceanog.2013.38>.
- Garcia-Pineda, O., Zimmer, B., Howard, M., Pichel, W., Li, X., MacDonald, I.R., 2009. Using SAR images to delineate ocean oil slicks with a texture-classifying neural network algorithm (TCNNA). *Can. J. Remote. Sens.* 35 (5), 1–11.
- Goodman, R., 1994. Overview and future trends in oil spill remote sensing. *Spill Science and Technology* 1 (1), 11–21.
- Grüner, K., Reuter, R., Smid, H., 1991. A new sensor system for airborne measurements of maritime pollution and of hydrographic parameters. *Geojournal* 24 (1), 103–117.
- Hurford, N., 1989. In: Lodge, A.E. (Ed.), *Review of Remote Sensing Technology, The Remote Sensing of Oil Slicks*. John Wiley and Sons, Chichester, UK, pp. 7–16.
- Hutchinson, G.E., 1957. *A treatise on limnology. Geography, Physics and Chemistry Vol-1*. John Wiley & Sons (1015 pp.).
- Jha, M.N., Levy, J., Gao, Y., 2008. Advances in remote sensing for oil spill disaster management: state-of-the-art sensors technology for oil spill surveillance. *Sensors* 8, 236–255.
- Lehr, B., Sky, B., Possolo, A., et al., 2010. Oil budget calculator Deepwater Horizon: A report to the National Incident Command. NOAA.
- Leifer, I., Lehr, W., Simecek-Beatty, D., Bradley, E., Clark, R., Dennison, P., Hu, Y., Matheson, S., Jones, C., Holt, B., Reif, M., Roberts, D., Svejkovsky, J., Swayze, G., Wozencraft, J., 2012. State of the art satellite and airborne marine oil spill remote sensing: application to the BP Deepwater Horizon oil spill. *Remote Sens. Environ.* 124, 185–209.
- Minchew, B., Jones, C.E., Holt, B., 2012. Polarimetric analysis of backscatter from the Deepwater Horizon oil spill using L-Band synthetic aperture radar. *IEEE Trans. Geosci. Remote Sens.* 50, 3812–3830.
- NOAA, 2011. URL: http://response.restoration.noaa.gov/faq_topic.php?faq_topic_id=1#2.
- NOAA, 2012. Open Water Oil Identification Job Aid for Aerial Observation. New Standardized Oil Slick Appearance and Structure Nomenclature and Code. NOAA Office of Response and Restoration, Emergency Response Division, Seattle, Washington (47 pp.).
- Peterson, C.H., et al., 2012. A tale of two spills: novel science and policy implications of an emerging new oil spill model. *Bioscience* 62 (5), 461–469 (2012).
- Rye, H., 2001. Probable effects of Langmuir circulation observed on oil slicks in the field. *Spill Sci. Technol. Bull.* 6 (3/4), 263–271.
- Shih, W.-C., Andrews, A.B., 2008. Modeling of thickness dependent thermal contrast of native and crude oil covered water surfaces. *Opt. Express* 16 (14), 10535–10542.
- Svejkovsky, J., Muskat, J., 2006. Real-time detection of oil slick thickness patterns with a portable multispectral sensor. Final Report for U. S. Minerals Management Service Contract 0105CT39144 (37 pp.).
- Svejkovsky, J., Muskat, J., 2009. Development of a portable multispectral aerial sensor for real-time oil spill thickness mapping in coastal and offshore waters. Final Report for U. S. Minerals Management Service Contract M07PC13205 (33 pp.).
- Svejkovsky, J., Muskat, J., 2012B. Open water multispectral aerial sensor oil spill thickness mapping in Arctic and high sediment load conditions. Final Report for Bureau of Safety and Environmental Enforcement Contract M10PC00068.
- Svejkovsky, J., Lehr, W., Muskat, J., Graettinger, G., Mullin, J., 2012A. Operational utilization of aerial remote sensing during oil spill response: lessons learned during the Deepwater Horizon spill. *Photogramm. Eng. Remote Sens.* 78 (10), 1089–1102.
- Svejkovsky, J., Muskat, J., Mullin, J., 2008. Mapping oil spill thickness with a portable multispectral aerial imager. *Proc. International Oil Spill Conference 2008* (4–8 May, 2008, Savannah, Georgia, unpaginated USB flash drive).
- Svejkovsky, J., Muskat, J., Mullin, J., 2009. Adding a multispectral aerial system to the oil spill response arsenal. *Sea Technol.* 50 (8), 17–22 (August 2009).
- Tseng, W.Y., Chiu, L.S., 1994. AVHRR observations of Persian Gulf oil spills. *Geoscience and Remote Sensing Symposium. IGARRS '94. Surface and atmosphere remote sensing: Technologies, data analysis and interpretation*. pp. 779–782.